The magnetic structure of $YMnO_3$ perovskite revisited

2002 J. Phys.: Condens. Matter 14 3285

(http://iopscience.iop.org/0953-8984/14/12/315)

INSTITUTE OF PHYSICS PUBLISHING JOURNAL OF PHYSICS: CONDENSED MATTER

J. Phys.: Condens. Matter **14** (2002) 3285–3294 PII: S0953-8984(02)31703-X

The magnetic structure of $YMnO_3$ perovskite revisited

A Muñoz[1], J A Alonso[2], M T Casais[2], M J Martínez-Lope[2], J L Martínez[2] and M T Fernández-Díaz[3]

[1] Depto de Física, EPS, Universidad Carlos III, Avda de la Universidad 30, Leganés-Madrid E-28911, Spain
[2] Instituto de Ciencia de Materiales de Madrid, CSIC, Cantoblanco, E-28049 Madrid, Spain
[3] Institut Laue-Langevin, BP 156X, 38042 Grenoble Cédex 9, France

E-mail: amunoz@fis.uc3m.es

Received 5 December 2001, in final form 24 January 2002
Published 15 March 2002
Online at stacks.iop.org/JPhysCM/14/3285

Abstract

The magnetic structure of the orthorhombic perovskite $YMnO_3$ has been investigated. A study on a polycrystalline sample based on neutron diffraction data and magnetization measurements has shown that $YMnO_3$ becomes magnetically ordered below $T_N = 42$ K. In the space group $Pnma$, the sinusoidal magnetic structure is defined by a $(C_x, 0, 0)$ mode and characterized by the propagation vector $\boldsymbol{k} = (k_x, 0, 0)$. The k_x-component increases from 0.420(4), immediately below the ordering temperature, to 0.435(2) at $T = 28.7$ K. Below 28 K the k_x-component remains unchanged. The sinusoidal spin arrangement remains stable down to 1.7 K; at this temperature the amplitude of the sinusoid is $A_k = 3.89(6)\ \mu_B$. $YMnO_3$ is the most distorted perovskite of the $RMnO_3$ series (R = rare earths); the observed sinusoidal magnetic structure is in contrast with those exhibited by the less-distorted members (i.e. $LaMnO_3$), which are commensurate-type antiferromagnetic structures.

1. Introduction

In recent years, the members of the $RMnO_3$ (R = rare earths) perovskite family have become the focus of many studies, since they are the parent compounds of the hole-doped oxides $R_{1-x}A_xMnO_3$ (A = alkaline earth) showing colossal-magnetoresistance properties [1–6]. In fact, the perovskite structure is observed for the $RMnO_3$ oxides with large-sized R^{3+} cations ($r_{R^{3+}} \geqslant r_{Dy^{3+}}$); these compounds adopt an orthorhombic structure, defined by the space group $Pnma$ (b is the longest axis) [7]. For R^{3+} cations smaller than Tb^{3+}, under ordinary synthesis conditions, $RMnO_3$ oxides crystallize in a hexagonal non-perovskite structure, of space group $P6_3cm$ [8]. The hexagonal compounds can be transformed to the perovskite form under high-pressure and high-temperature conditions [9], although in some cases, for R = Ho, Er, Y, the

perovskite structure is metastable under ambient conditions and can be synthesized by soft-chemistry procedures [10–12]. The difficulty of preparation of $YMnO_3$ in its perovskite form accounts for the relative scarcity of reports devoted to the description of its basic properties.

In the $RMnO_3$ perovskite structure, the Mn^{3+} d^4 levels are split by the oxygen octahedral crystal field into a lower-energy t_{2g} triplet and a higher-energy e_g doublet, which are filled according to Hund's rules giving rise to the electron configuration $t_{2g}^3 e_g^1$. The Jahn–Teller character of the Mn^{3+} cations lies at the origin of the strong distortion of the MnO_6 octahedra and it leads to an orbital ordering in the *a*–*c* plane (space group *Pnma*) [13–15]. This Jahn–Teller distortion is present for all the $RMnO_3$ compounds; the distortion slightly increases from La to Tb and remains nearly unchanged for Ho, Er and Y [16].

The magnetic properties and spin arrangements in $RMnO_3$ were initially analysed a long time ago [17–21]. The ordering temperature for the Mn ions decreases with the R ionic radius, ranging from $T_N = 141$ K for La to 40 K for Tb; for R = Ho, Y and Er the ordering temperature is around 40 K. The R^{3+} cations also become magnetically ordered, but at lower temperatures [19, 22]. As regards the magnetic structure, neutron diffraction experiments have shown that $LaMnO_3$ orders with an antiferromagnetic C-type structure (*Pnma* setting), consisting of ferromagnetic *a*–*c* layers antiferromagnetically coupled along the *b*-direction [18, 23, 24]. A similar magnetic structure was found for $PrMnO_3$ and $NdMnO_3$ [19], although for this last compound a ferromagnetic component associated with the Mn ions seems to be present along the *b*-direction [25]. The stable magnetic structures for heavier rare earths seem to be incommensurable, since $TbMnO_3$ orders with a sinusoidal-wave magnetic structure defined by the propagation vector $\boldsymbol{k} = (k_x, 0, 0)$ [26] and $HoMnO_3$ also undergoes magnetic ordering below 40 K with a sinusoidal-wave magnetic structure defined by a similar propagation vector [27]. For this last compound, the magnetic structure has the particularity of becoming commensurable with $\boldsymbol{k} = (1/2, 0, 0)$ below 26 K [28]. In both cases, below the ordering temperature, the spin arrangement for the Mn ions is given by the magnetic mode $(C_x, 0, 0)$. For the larger rare-earth perovskites (La, Pr and Nd) the Mn magnetic moments are also oriented along the *a*-axis direction [18, 19, 23–25]. In this coherent scenario, the reported magnetic structure of $YMnO_3$ is singular in the sense that magnetic orientation for the Mn magnetic moments has been described as helical, with the moments rotating in the *b*–*c* plane and defined by the magnetic mode $(0, C_x, C_z)$. The aim of this paper is to revise the $YMnO_3$ magnetic structure and analyse its thermal evolution from powder neutron diffraction data. In order to complete this study, magnetic measurements will also be presented.

2. Experimental procedures

Orthorhombic $YMnO_3$ was prepared from citrate precursors obtained by soft-chemistry procedures. Stoichiometric amounts of analytical grade Y_2O_3 and $MnCO_3$ were dissolved in citric acid, then the solution was slowly evaporated, dried at 120 °C and then slowly decomposed at temperatures up to 700 °C. The yield of the orthorhombic phase could be optimized by annealing the precursor powders in an O_2 flow at 900 °C for 12 h, thus minimizing the stabilization of the competitive hexagonal $YMnO_3$ phase. The product was initially characterized by laboratory XRD for phase identification and to assess phase purity. The oxygen content of the sample was determined by thermal analysis in reducing conditions (H_2/N_2 flow), through total reduction to $MnO + R_2O_3$.

The magnetic measurements were carried out in a commercial SQUID magnetometer. The DC susceptibility was measured under a 5 kOe magnetic field for temperatures ranging

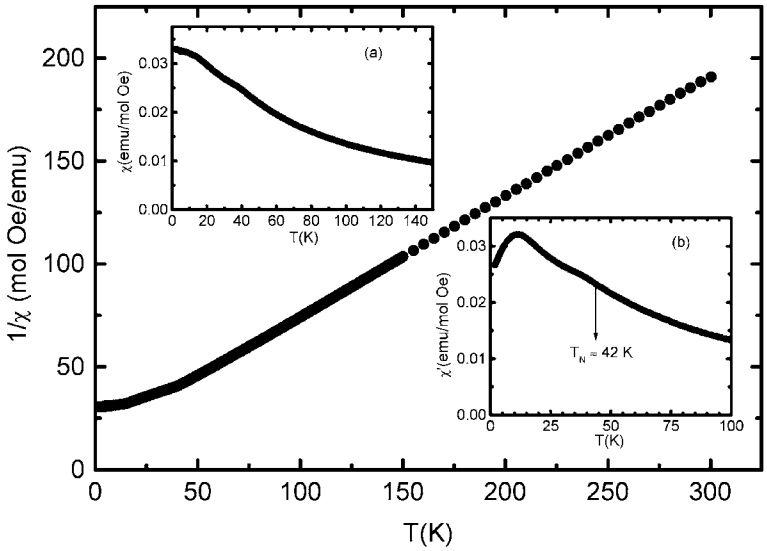

Figure 1. Thermal evolution of the inverse of the DC susceptibility measured under a 5 kOe applied magnetic field. Insets: (a) thermal variation of the DC susceptibility; (b) thermal evolution of the real part of the AC susceptibility.

from 2 to 300 K. The AC susceptibility was recorded in an oscillating magnetic field at 997 Hz in the temperature interval $1.7 < T < 275$ K. Isothermal magnetization curves were obtained at $T = 2$, 5, 20 and 50 K in the magnetic field interval $-50 < H < 50$ kOe interval. Specific heat measurements were also obtained in a semiadiabatic He calorimeter by using the heat-pulse-relaxation method under a zero magnetic field in the temperature range $2 < T < 100$ K. Neutron powder diffraction (NPD) patterns were collected at the Institut Laue-Langevin in Grenoble (France), at the D20 high-flux diffractometer. A set of NPD diagrams were obtained with a wavelength $\lambda = 2.42$ Å in the temperature range from 1.7 to 271 K. The refinements of both crystal and magnetic structures were performed by the Rietveld method with the FULLPROF code [29]. In the refinements, the peak shape was simulated by a pseudo-Voigt function and the background was fitted with a fifth-degree polynomial function.

3. Results

$YMnO_3$ was obtained as a black, well crystallized powder. The determination of the oxygen content leads to the formula $YMnO_{3.04(1)}$, suggesting a slight oxygen excess which implies a measurable Mn^{4+} content of 8%, probably inherent to the stabilization of the orthorhombic phase in O_2 flow. Also, a significant amount of the competitive hexagonal phase of the same stoichiometry was observed in the diffraction patterns. The main phase of the XRD and neutron diagrams was indexed in the conventional *Pnma* orthorhombic model, with unit-cell parameters related to a_0 (ideal cubic perovskite, $a_0 \approx 4$ Å) as $a \approx \sqrt{2}a_0$, $b \approx 2a_0$, $a \approx \sqrt{2}a_0$.

3.1. Magnetic measurements

The thermal evolution of the DC magnetic susceptibility is shown in figure 1. Above $T = 100$ K the reciprocal susceptibility follows the Curie–Weiss law, with the effective paramagnetic moment of 3.69(1) μ_B per formula unit (fu) and the characteristic paramagnetic temperature

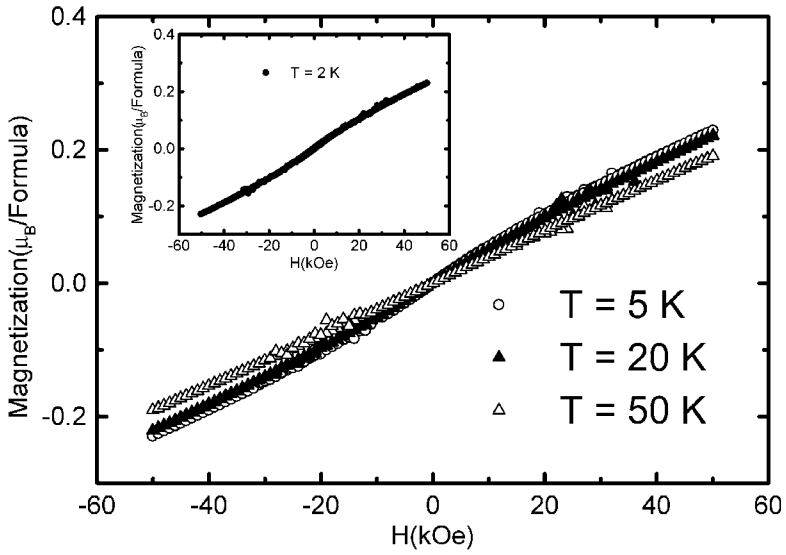

Figure 2. Cyclic isothermal magnetization curves. Inset: for $T = 2$ K.

$\Theta_P = -26(1)$ K. The effective paramagnetic moment is below the expected value for the high-spin Mn^{3+} ion in the ground state, 4.90 μ_B. The inset (a) of figure 1 shows a subtle kink in the susceptibility curve at around 40 K, which could indicate the appearance of a long-range magnetic order. This effect is more clearly observed at around 42 K in the real part of the AC susceptibility curve, presented in the inset (b) of figure 1. Furthermore, in the specific heat measurements carried out on this sample, a sharp anomaly is observed at 42 K, which confirms the appearance of a magnetic ordering with $T_N = 42$ K. This temperature value coincides with the reported ordering temperature for $YMnO_3$ [21]. On the other hand, the AC susceptibility exhibits a maximum at around $T = 11$ K, that can be related to a characteristic freezing temperature associated with the partial spin-glass behaviour of the sample. In the isothermal magnetization curves, reported in figure 2, below the ordering temperature, neither a remnant magnetization nor hysteresis phenomena are observed. At $T = 50$ K, above the ordering temperature, the magnetization curve presents a linear behaviour.

3.2. Neutron diffraction measurements

The crystal structure was refined from a NPD pattern obtained at 275 K, with $\lambda = 2.42$ Å. The lattice parameters were $a = 5.970(9)$ Å, $b = 7.3606(11)$ Å and $c = 5.2404(9)$ Å, in the orthorhombic space group $Pnma$. As shown in figure 3(*b*), additional Bragg peaks are present in the diagram, corresponding to minor impurities of the hexagonal phase of $YMnO_3$ (space group $P6_3cm$). In the final fitting of the NPD pattern, both phases were taken into consideration. For the orthorhombic phase, the atomic positions were those reported in [16], obtained from a high-resolution NPD study performed on the same sample.

For the hexagonal phase, the atomic positions were taken from [30]. From the relative scale factors, the amount of hexagonal phase is 10.1(7)%, in good agreement with the results presented in [16]. The mean structural parameters of the Rietveld refinement are presented in table 1, and figure 3(*b*) illustrates the quality of the fit.

The NPD patterns collected in the temperature range $1.7 < T < 275$ K have shown that below $T = 44.4$ K new reflections are observed at 2θ angles not allowed for the Bragg

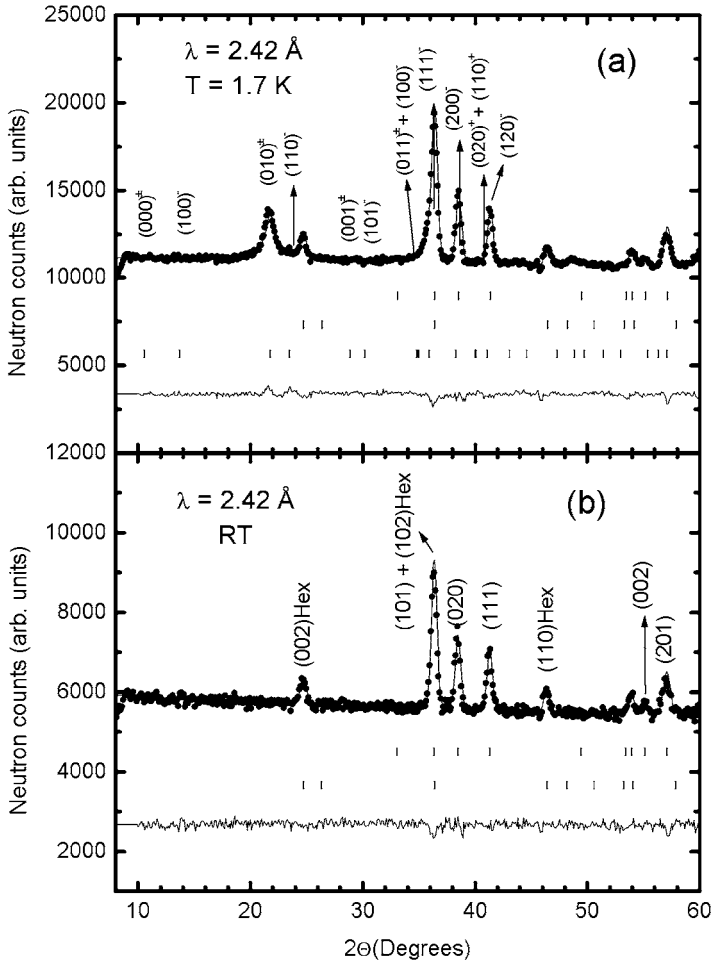

Figure 3. Observed (solid circles), calculated (continuous curve) and difference (continuous curve) NPD patterns. (*a*) Fitting of the magnetic structure. The Bragg reflections are indicated by tick marks: first row (orthorhombic phase (nuclear)), second row (hexagonal phase (nuclear)) and third row (orthorhombic (magnetic peaks)). (*b*) Fitting of the crystallographic structure. Tick marks: first row: orthorhombic phase; second row: hexagonal phase.

positions in the space group $Pnma$. This reveals the appearance of a magnetic ordering in good agreement with the anomalies observed in the specific heat and AC susceptibility measurements. All of the magnetic peaks can be indexed with a propagation vector $\boldsymbol{k} = (k_x, 0, 0)$. The magnetic satellites only appear at (hkl) reciprocal-lattice points with $k = 2n+1$ and $h + l = 2n$. This is in good agreement with the previous neutron diffraction results presented by Quezel *et al* [11]. In that work, the space group is $Pbnm$ (c is the longest axis), the propagation vector is $\boldsymbol{k}' = (0, k_y, 0)$ and the extinction rules are $h'+k' = 2n$ and $l' = 2n+1$. On decreasing the temperature below 44.4 K, no changes are observed in the NPD diagrams that could suggest a transition to another magnetic phase, except an increase in the intensity of the magnetic reflections, as illustrated for the $(010)^{\pm}$ satellite in figure 4(*a*).

A feature which must be underlined is the slight change of the angular positions of the magnetic satellites with temperature, implying a variation in the k_x-component of the magnetic

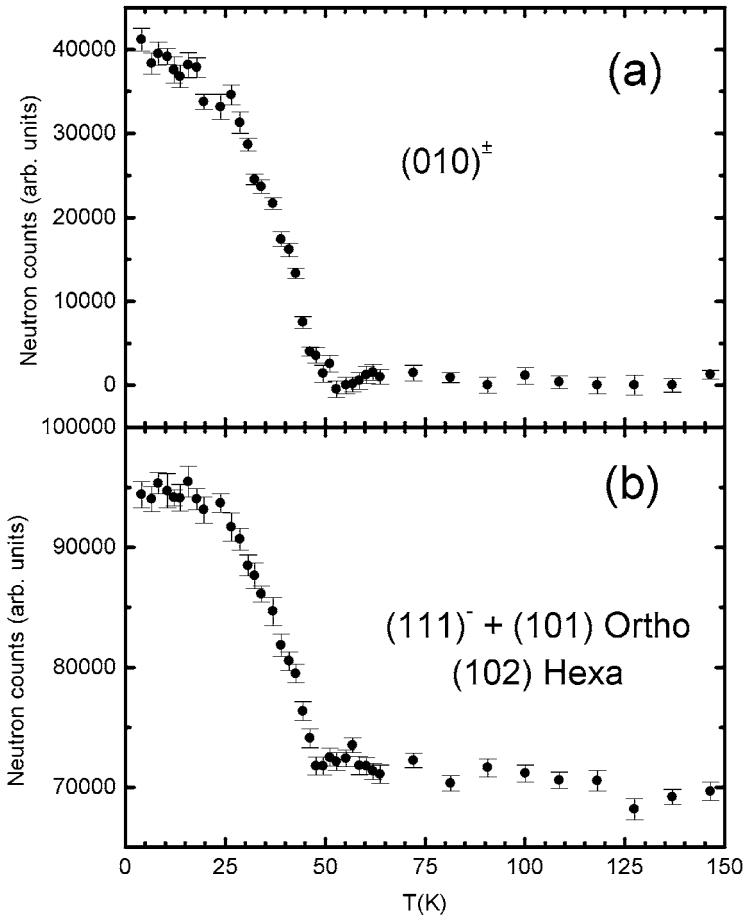

Figure 4. Thermal evolution of the integrated intensity of different magnetic peaks.

Table 1. Structural parameters used for the Rietveld refinement of the NPD patterns at room temperature and with $\lambda = 2.42$ Å. The atomic positions are those reported in [16]. Space group *Pnma*.

Atoms	Positions	*x*	*y*	*z*
Y	4c	0.0855	0.2500	0.9819
Mn	4b	0.0000	0.0000	0.5000
O1	4c	0.4660	0.2500	0.1093
O2	8d	0.3266	0.0520	0.7005
Cell dimensions (orthorhombic) (Å)	$a = 5.7970(9)$	$b = 7.3606(11)$	$c = 5.2404(9)$	
Cell dimensions (hexagonal) (Å)	$a = b = 6.156(3)$	$c = 11.350(7)$	Amount = 10.1(7)%	
Discrepancy factor	R_{Bragg} (orthorhombic) = 5.5%	R_{Bragg} (hexagonal) = 8.7%	$\chi^2 = 1.9$	

propagation vector. As shown in figure 5, $k_x = 0.420(4)$ at $T = 44.4$ K, and as the temperature decreases, k_x sharply increases, taking a value of $k_x = 0.4361(13)$ at 28 K, which remains constant down to $T = 1.7$ K. These k_x-values are very different from that given in [11], of 0.0786.

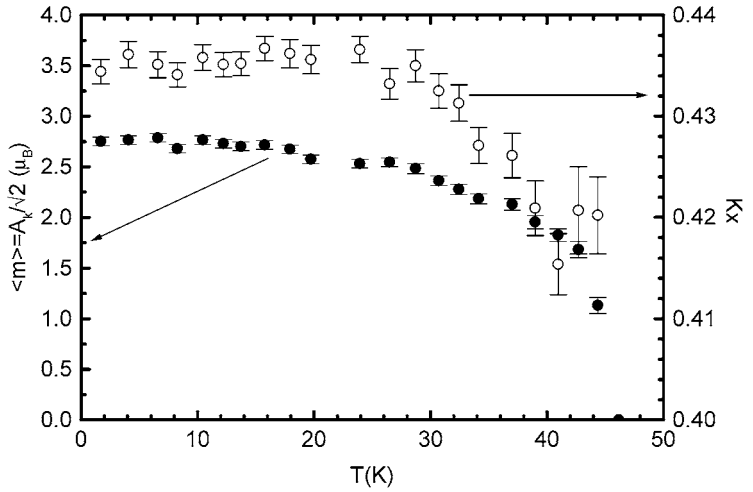

Figure 5. Right axis: thermal variation of the mean value of the magnetic moment. A_k is the amplitude of the sinusoid. Left axis: thermal variation of the k_x-component of the propagation vector.

The magnetic ordering of the minor hexagonal phase is not observed in the NPD patterns. Hexagonal $YMnO_3$ has been reported to order at $T_N \approx 70$ K with a magnetic structure defined by the propagation vector $\boldsymbol{k} = 0$, with (100), (101) and (102) the strongest magnetic reflections [30]. On the one hand, an increase of the intensity of the hexagonal reflection (102) below 70 K is not appreciated in figure 4(*b*), and, on the other hand, the reflections (100) ($2\Theta_{exp} = 26.37^\circ$) and (101) ($2\Theta_{exp} = 29.18^\circ$) are not observed at $T = 1.7$ K (see figure 3(*b*)).

3.3. Magnetic structure of $YMnO_3$ perovskite

The possible magnetic modes compatible with the symmetry of the $YMnO_3$ perovskite, determined according to the group theory analysis, were presented in [28]. After checking the different solutions, the one most compatible with the experimental data is a sinusoidal magnetic structure given by the (C_x, 0, 0) magnetic mode (*Pnma* setting). This implies that the magnetic moments of the Mn^{3+} ions are oriented along the x-direction, parallel to the modulation direction. The four Mn^{3+} ions in the unit cell, denoted by 1, 2, 3 and 4, occupy the (0, 0, 1/2), (1/2, 0, 0), (0, 1/2, 1/2) and (1/2, 1/2, 0) atomic positions, respectively. For the C_x-mode the relationships among the Fourier components of the different magnetic moments of the Mn^{3+} ions are $m^{\boldsymbol{k}}_{1x} = e^{i\pi k_x} m^{\boldsymbol{k}}_{2x} = -m^{\boldsymbol{k}}_{3x} = -e^{i\pi k_x} m^{\boldsymbol{k}}_{4x}$. This solution remains stable in the $1.7 \leqslant T \leqslant 44$ K temperature range.

The good agreement between the experimental and calculated patterns for the sinusoidal wave can be seen in figure 3(*b*), for $T = 1.7$ K. The thermal evolution of the mean value of the magnetic moment is presented in figure 5. At $T = 1.7$ K the amplitude of the sinusoid is 3.89(6) μ_B, which corresponds to a mean value for the moment of 2.75(4) μ_B (see table 2). A plot of the magnetic structure is reported in figure 6. The most important parameters of the refinement at $T = 1.7$ K are presented in table 2.

The magnetic structure found in this study is in sharp contrast with the magnetic structure previously reported in [11]. According to the former work, the magnetic structure is helical with the magnetic moments placed in the *b*–*c* plane (*Pnma* setting). After testing this solution, the agreement with the experimental data is clearly worse ($R_{Bragg} = 14.8\%$) than that obtained with the present sinusoidal solution ($R_{Bragg} = 4.1\%$).

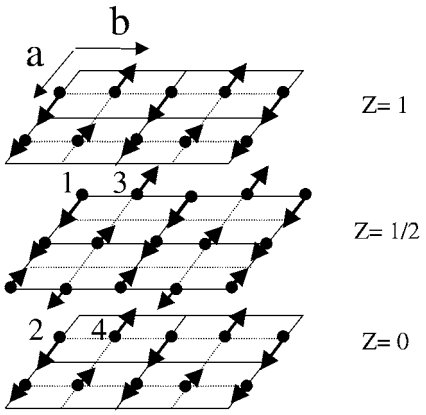

Figure 6. A schematic view of the magnetic structure of $YMnO_3$.

Table 2. Magnetic structure refinement from a NPD pattern at $T = 1.7$ K and $\lambda = 2.42$ Å.

Solution,	m_x^k,	$m_x^k/\sqrt{2}$,	k_x,
$(C_x, 0, 0)$	3.89(6) μ_B	2.75(4) μ_B	0.4344(12)

Discrepancy factor R_{Bragg} (orthorhombic) = 4.1% R_{Bragg} (hexagonal) = 5.0% R_{Bragg} (mag) = 5.3% $\chi^2 = 2.0$

4. Discussion

Neutron diffraction measurements have confirmed that $YMnO_3$ adopts an antiferromagnetic ordering below $T_N = 42$ K. The magnetic structure is sinusoidally modulated with the magnetic moments of the Mn^{3+} ions oriented parallel to the propagation vector $\boldsymbol{k} = (k_x, 0, 0)$ and it remains stable and incommensurable down to 1.7 K. However, the propagation vector undergoes a thermal variation: at $T = 44.4$ K, $k_x = 0.420$, and it increases up to $k_x = 0.435$ at around 28 K; below this temperature there are no further changes.

On the other hand, the transition from the paramagnetic state to the ordered state clearly appears in the AC susceptibility curve as a change of slope, although the temperature at which the propagation vector is blocked is not observed. In the DC susceptibility the magnetic ordering transition appears as a subtle kink in the curve, at around 40 K. The effective magnetic moment obtained from the reciprocal susceptibility, $\mu_{eff} = 3.69\ \mu_B$, is below the expected value for spin-only Mn^{3+} ions ($S = 2$, $\mu_{calc} = 4.90\ \mu_B$); this could be a result of covalency effects, and also can be understood by considering that a significant content of Mn^{4+} ($S = 3/2$) is present in the sample, as was pointed out in [16] (it was estimated, from the determination of the oxygen content by thermal analysis, that the amount of Mn^{4+} is around 8%). This was a consequence of the stabilization process of the orthorhombic phase. At the same time, the presence of the Mn^{4+} ions introduces some disorder in the lattice and this could be the origin of some spin-glass features observed in the AC susceptibility at low temperature, showing a maximum at 11 K which would correspond to the freezing temperature of the spin glass.

As a common feature of the three last of the perovskite $RMnO_3$ series (R = Tb, Ho, Y), the magnetically ordered state for the Mn^{3+} ions below T_N seems to be a sinusoidal magnetic structure defined by the magnetic mode $(C_x, 0, 0)$, and characterized by the propagation vector $\boldsymbol{k} = (k_x, 0, 0)$. This is in contrast with the commensurable ($\boldsymbol{k} = 0$) magnetic

structure exhibited by the lighter members of the series (R = La, Pr, Nd), that consists of ferromagnetic *a–c* layers antiferromagnetically coupled along the *b*-direction (in the *Pnma* setting). This ordering is associated with the orbital ordering of the e_g orbitals within each layer, originated by the cooperative Jahn–Teller distortion of the MnO_6 octahedra. According to the Goodenough–Kanamori [31] rules, the Mn–O–Mn superexchange interaction in the *a–c* layer through the e_g orbitals is ferromagnetic, while the interaction along the *b*-direction, which takes place through the t_{2g} orbitals, is antiferromagnetic. In spite of the observed differences in magnetic structure between the light and heavy members of the series, there are some common features. On one hand, the magnetic anisotropy tends to align the magnetic moments along the *a*-direction for all of them; on the other hand, the magnetic interaction along the *b*-direction is antiferromagnetic. The differences in magnetic structure between the two ends of the $RMnO_3$ series concern the spin arrangement in the *a–c* plane, even though the orbital ordering originated by the Jahn–Teller effect is present in all of the compounds of the series [16]. As has been shown for $HoMnO_3$ [27, 28], and within the classical framework of the Heisenberg Hamiltonian, the existence of an incommensurate magnetic structure requires that the superexchange parameters associated with the Mn–O–O–Mn exchange path along the *a*-direction are taken into consideration, together with the nearest-neighbour exchange parameters associated with the Mn–O–Mn interaction. This implies that the nearest-neighbour exchange parameters are smaller for the heavier compounds of the series. There are two facts that reinforce this assumption: firstly, the ordering temperature is smaller for the heavier compounds (T_N = 130 K for $LaMnO_3$ versus 42 K for $YMnO_3$); and secondly, the distortion of the MnO_6 octahedra and the deviation of the ⟨Mn–O–Mn⟩ bonding angle with respect to 180°, are greater for R = Tb, Ho and Y [16]. For $YMnO_3$, the average Mn–O–Mn angle can be as low as 146°. For such a distorted framework, the overlapping between 3d Mn and 2p O orbitals is not large enough to provide a superexchange ferromagnetic interaction between neighbouring Mn cations within each *a–c* layer, as happens in $LaMnO_3$. For $YMnO_3$, the nearest-neighbour exchange parameters are much weaker than those found for $LaMnO_3$—such that next-nearest-neighbour parameters become important and account for the incommensurability of the magnetic structure.

5. Conclusions

Neutron diffraction measurements have shown that the orthorhombic $YMnO_3$ perovskite presents a sinusoidal magnetic structure below T_N = 42 K, defined by the magnetic mode $(C_x, 0, 0)$ and characterized by the propagation vector $\boldsymbol{k} = (k_x, 0, 0)$. This spin arrangement is a common feature for the heavier, more distorted perovskites of the $RMnO_3$ series (R = Tb, Ho, Y) below the magnetic ordering temperature. In $YMnO_3$, the sinusoidal magnetic structure remains stable down to 1.7 K, although some subtle changes are observed in the propagation vector. The k_x-component increases from 0.420(4) below the ordering temperature up to 0.435(2) at T = 8.7 K. Below 28 K the k_x-component is blocked at around 0.435. The results obtained in the magnetic measurements are in good agreement with the onset of magnetic ordering obtained from neutron diffraction measurements. The AC susceptibility curve could suggest the existence of a spin-glass behaviour below 11 K, which has been associated with the disorder of the lattice introduced by the presence of Mn^{4+} ions, which seem to be necessary for the stabilization of the orthorhombic versus the competitive hexagonal $YMnO_3$ phase.

References

[1] Kusters R M, Singleton J, Keen D A, McGreevy R and Hayes W 1989 *Physica* B **155** 362
[2] Von Helmolt R, Wecker J, Holzapfel B, Schultz L and Samwer K 1993 *Phys. Rev. Lett.* **71** 2331
[3] Tokura Y, Urushibara A, Morimoto Y, Arima T, Asamitsu A, Kido G and Furukawa N 1994 *J. Phys. Soc. Japan* **63** 3931
[4] Kuwahara H, Tomioka Y, Asamitsu A, Moritomo Y and Tokura Y 1995 *Science* **270** 961
[5] Tomioka Y, Asamitsu A, Kuwahara H, Moritomo Y and Tokura Y 1996 *Phys. Rev.* B **53** R1689
[6] Yoshizawa H, Kawano H, Tomioka Y and Tokura Y 1996 *J. Phys. Soc. Japan* **65** 1043
[7] Gilleo M A 1957 *Acta Crystallogr.* **10** 161
[8] Yakel H, Koehler W C, Bertaut E F and Forrat F 1963 *Acta Crystallogr.* **16** 957
[9] Waintal A and Chenavas J 1967 *Mater. Res. Bull.* **2** 819
[10] Szabo G 1969 *PhD Thesis* Lyon University
[11] Quezel S, Rossat-Mignod J and Bertaut E F 1974 *Solid State Commun.* **14** 941
[12] Brinks H W, Fjellvag H and Kjekshus A 1997 *J. Solid State Chem.* **129** 334
[13] Solovyev I, Hamada N and Terakura K 1996 *Phys. Rev. Lett.* **76** 4825
[14] Mizokawa T and Fujimori A 1996 *Phys. Rev.* B **54** 5368
[15] Ishiara S, Inoue J and Maekawa S 1997 *Phys. Rev.* B **55** 8280
[16] Alonso J A, Martínez-Lope M J, Casais M T and Fernández-Díaz M T 2000 *Inorg. Chem.* **39** 917
[17] Jonker G H and Van Santen J H 1950 *Physica* **16** 337
Jonker G H and Van Santen J H 1953 *Physica* **19** 120
[18] Wollan E O and Koehler W C 1955 *Phys. Rev.* **100** 545
[19] Quezel-Ambrunaz S 1968 *Bull. Soc. Fr. Minér. Cristallogr.* **91** 339
[20] Pauthenet R and Veyret C 1970 *J. Physique* **31** 65
[21] Wood V E, Austin A E, Collings E W and Brog K C 1973 *J. Phys. Chem. Solids* **34** 859
[22] Troyanchuk Y, Kasper N V, Szymczak H and Nabialek A 1997 *Low Temp. Phys.* **23** 300
[23] Koehler W C and Wollan E 1957 *J. Phys. Chem. Solids* **2** 100
[24] Moussa F, Hennion M, Rodríguez-Carvajal R, Moudden H, Pinsard L and Revcolevschi A 1966 *Phys. Rev.* B **54** 15 149
[25] Muñoz A, Alonso J A, Martínez-Lope M J, García-Muñoz J L and Fernández-Díaz M T 2000 *J. Phys.: Condens. Matter* **12** 1361
[26] Quezel S, Tcheou F, Rossat-Mignod J, Quezel G and Roudaut E 1977 *Physica* B **86–8** 916
[27] Brinks H W, Rodríguez-Carvajal J, Fjellvag H, Kjekshus A and Hauback B 2001 *Phys. Rev.* B **63** 94 411
[28] Muñoz A, Casais M T, Alonso J A, Martínez-Lope M J, Martínez J L and Fernández-Díaz M T 2001 *Inorg. Chem.* **40** 1020
[29] Rodríguez-Carvajal J 1993 *Physica* B **192** 55
[30] Muñoz A, Alonso J A, Martínez-Lope M J, Casais M T, Martínez J L and Fernández-Díaz M T 2000 *Phys. Rev.* B **62** 9498
[31] Goodenough J B 1955 *Phys. Rev.* **100** 564